Sven Jachalke, Tony Schenk, Min Hyuk Park, Uwe Schroeder, Thomas Mikolajick, Hartmut Stöcker, Erik Mehner, Dirk C. Meyer

Pyroelectricity of silicon-doped hafnium oxide thin films

Erstveröffentlichung in / First published in:

Applied physics letters. 2018, 112(14), S. 142901-1 – 142901-5 {Zugriff am: 18.08.2021}. AIP Publishing. ISSN 1077-3118.

DOI: https://doi.org/10.1063/1.5023390

Applied Physics Letters

Pyroelectricity of silicon-doped hafnium oxide thin films

Cite as: Appl. Phys. Lett. **112**, 142901 (2018); https://doi.org/10.1063/1.5023390
Submitted: 23 January 2018 . Accepted: 17 March 2018 . Published Online: 02 April 2018

Sven Jachalke, Tony Schenk, Min Hyuk Park, Uwe Schroeder, Thomas Mikolajick, Hartmut Stöcker, Erik Mehner, and Dirk C. Meyer

Pyroelectricity of silicon-doped hafnium oxide thin films

Sven Jachalke,[1,a)] Tony Schenk,[2] Min Hyuk Park,[2] Uwe Schroeder,[2] Thomas Mikolajick,[2,3] Hartmut Stöcker,[1] Erik Mehner,[1] and Dirk C. Meyer[1]
[1]*Institute of Experimental Physics, TU Bergakademie Freiberg, Leipziger Str. 23, 09599 Freiberg, Germany*
[2]*NaMLab gGmbH, Nöthnitzer Str. 64, 01187 Dresden, Germany*
[3]*Institute for Semiconductors and Microsystems, TU Dresden, Nöthnitzer Str. 64, 01187 Dresden, Germany*

(Received 23 January 2018; accepted 17 March 2018; published online 2 April 2018)

Ferroelectricity in hafnium oxide thin films is known to be induced by various doping elements and in solid-solution with zirconia. While a wealth of studies is focused on their basic ferroelectric properties and memory applications, thorough studies of the related pyroelectric properties and their application potential are only rarely found. This work investigates the impact of Si doping on the phase composition and ferro- as well as pyroelectric properties of thin film capacitors. Dynamic hysteresis measurements and the field-free Sharp-Garn method were used to correlate the reported orthorhombic phase fractions with the remanent polarization and pyroelectric coefficient. Maximum values of 8.21 μC cm^{-2} and −46.2 μC K^{-1} m^{-2} for remanent polarization and pyroelectric coefficient were found for a Si content of 2.0 at%, respectively. Moreover, temperature-dependent measurements reveal nearly constant values for the pyroelectric coefficient and remanent polarization over the temperature range of 0 °C to 170 °C, which make the material a promising candidate for IR sensor and energy conversion applications beyond the commonly discussed use in memory applications. *Published by AIP Publishing.*
https://doi.org/10.1063/1.5023390

The report of ferroelectricity in hafnia-based thin films[1] revived the interest in ferroelectrics for memory applications.[2–7] This is mainly due to the fact that fluorite-type ferroelectrics[8,9] are fully compatible with state-of-the-art complementary metal-oxide-semiconductor (CMOS) technology. Moreover, the material composition is rather simple and a wealth of dopants has been shown to induce ferroelectric properties in hafnia[2,8,10–16] or zirconia.[17,18] This has been achieved via different deposition techniques including atomic layer deposition (ALD), which is very suitable for ultra-thin films of high quality even in 3D structures.[19] Also, cheaper chemical solution deposition has proven to be capable of producing ferroelectric films with thicknesses below 100 nm.[20] This opens up a wide field of applications beyond memory devices. Exploiting the related piezo- and pyroelectric properties is an obvious approach.[18,20–23] The investigations of pyroelectric properties of HfO_2, i.e., the change in its remanent polarization P_R with respect to a change in temperature T, lack comprehensive studies, especially with respect to the different doping possibilities of the material. The measurement of the pyroelectric coefficient p is typically composed of several contributions (see Ref. 24) and generally given by the change in dielectric displacement field D with temperature T, $p = \mathrm{d}D/\mathrm{d}T$. Its quantification is essential to estimate the usability of a material at varying temperatures. Park *et al.*[2,23] and Hoffmann *et al.*[22] recently demonstrated the potential of hafnia- and zirconia-based films for pyroelectric devices such as thin film IR sensors, waste heat energy converters, or electrocaloric cooling machines. Furthermore, Smith *et al.*[21] showed outstanding ferro- and pyroelectric properties in zirconium-doped hafnium oxide at room temperature. The variation of the ferroelectric properties due to the doping with silicon was first demonstrated by Böscke *et al.*,[1] followed by the works of Hoffmann *et al.*[22] and Richter *et al.*[25] An investigation on its related piezo- and pyroelectric properties is still pending. This is where the present study comes into play, while another very recent work investigated the impact of thickness and field-cycling stability for a fixed Si content.[26] While both are important parameters, the dependence on compositional changes is also of particular importance for future applications and device manufacturing and, thus, subject of this work.

Capacitors formed by approximately 12 nm thick Si:HfO_2 sandwiched between 12 nm thick TiN top and bottom electrodes were fabricated as described elsewhere.[25] The Si content was adjusted by varying the ratio of HfO_2 to SiO_2 cycles during ALD between 30:1 and 8:1. This resulted in a Si concentration between 1.6 at% and 3.8 at% (at%, i.e., Si/[Hf + Si + O]) as determined by time-of-flight secondary ion mass spectrometry and outlined previously.[25] The corresponding cationic ratios Si/[Si + Hf], as commonly used in publications other than Ref. 25, are 3.2 cat% and 11.1 cat%. All samples were annealed in a nitrogen atmosphere for 20 s at 800 °C to crystallize the capacitor stacks.

Ferroelectric hysteresis measurements were performed using the shunt method in order to characterize the polarization state of the samples. Here, the charging current I of the capacitors is recorded from the voltage drop V over a well-known reference resistor R during the continuous cycling of an applied electric field E (for more information, see Ref. 27). Integrating the current $I(t)$ yields $P = 1/A \times \int I(t)\,\mathrm{d}t$ since it equals the corresponding charge divided by the contact area A. The axis intercepts of the P–E hysteresis correspond to the coercive field strength E_C and remanent polarization P_R. The value of P_R was measured after 10^3 to 10^4 cycles in order to minimize influences of the wake-up and fatigue effects.[28–31]

For the characterization of the pyroelectric coefficient p and its temperature dependency, the Sharp-Garn method[32,33] utilizing a sinusoidal temperature excitation of the sample, while simultaneously measuring the compensational current

a)Electronic mail: sven.jachalke@physik.tu-freiberg.de

flow, was used. Compared to a temperature-dependent measurement of P_R from the ferroelectric hysteresis, this method operates without an external electric field. From the contact area A, excitation frequency f, temperature and current amplitude, T_A and I_A, and phase shift ϕ between temperature and current oscillation, the pyroelectric coefficient is given by $p = I_A \times \sin(\phi)/(T_A \times A \times 2\pi f)$. Here, ϕ is an indicator for a pyroelectric ($\phi = 90°$) or non-pyroelectric ($\phi = 0°$) signature. Continuously shifting the offset, realized by superimposing the oscillations with a linear function, allows determining $p(T)$ in the range of 0 °C to 170 °C. The actual temperature course and measured current signal are exemplified in Fig. SI (see supplementary material SI) and are qualitatively similar for all samples. The used measurement setup is described elsewhere.[24] The upper contact pad was connected by a tungsten needle, and the bottom connection was established with the help of silver conductive paint at the wafer edge. Furthermore, an HP 4284A precision LCR meter was used to determine the dielectric constant ε_r of the samples, which, besides p, is necessary to calculate the figures of merit for energy harvesting and IR sensor applications (for details, see supplementary material SII and SIII). The actual pad size for each sample was determined from microscopy images and amounts to approx. 0.15 mm^2. A temperature amplitude of 2 K, a frequency of 10 mHz, and a heating rate of 25 Kh^{-1} were used for the thermal stimulation. The error of p is estimated from the statistical errors of fitted signals and the pad area at the 1σ level.

The evolution of the hysteresis with the increasing Si concentration is summarized in Fig. 1. It shows typical non-polar (orange), ferro- (blue), and antiferroelectric (green background) shapes depending on the Si concentration, which is in good agreement with recent results.[22,25] It has been argued before[25,34] that field-induced ferroelectricity is a more general and more appropriate description for the double-hysteresis loops compared to the original definition of antiferroelectricity by Kittel.[35] In recent years, however, the term antiferroelectricity has commonly been used in a wider sense[2,8,25,26,34,36] including the present case of a transition from a non-polar tetragonal to a polar orthorhombic phase. Therefore, and for the sake of convenience, the term antiferroelectricity is used in accordance with this wider sense in the following. Ferroelectricity is obtained for Si concentrations from approx. 1.9 at% to 2.5 at%, while antiferroelectric behavior exists for Si concentrations of around 2.5 at% to 3.5 at%. Below 2.0 at% and above 3.5 at%, the linear dielectric P–E shape reveals the non-polar character of the layer. The resulting values of P_R from the axis intercepts are shown in Fig. 2 with respect to the Si concentration. Also, the values of the pyroelectric coefficient p at room temperature determined using the Sharp-Garn method are provided. The comparison between the untreated sample, poled after a P–E measurement, and after heating during a $p(T)$ measurement shows the differences due to thermal treatment and poling. Furthermore, figures of merit F_E and F_I, often used to assess the usability of a material for energy harvesting and IR sensor applications are shown (for further details, see supplementary material SIII), respectively. Fitted fractions of the monoclinic (space group $P2_1/c$), orthorhombic ($Pca2_1$), and tetragonal ($P4_2/nmc$) phases obtained from Rietveld refinement according to Park *et al.*[8] are also given in Fig. 2.

P_R and p rise and fall simultaneously, depending on the Si concentration peaking at an Si concentration of 2.0 at% with maximum values of $-46.2(6.1)$ µC K^{-1} m^{-2} and $8.21(0.22)$ µC cm^{-2}, respectively. Accordingly, the maximum figures of merit are $k^2 = 8.71(1.56)$, $F_E = 7.64(1.37)$ J m^{-3} K^{-1}, $F'_E = 11.03(1.98) \times 10^{-12}$ m^3 J^{-1}, $F_I = 17.55(1.05)$ m V^{-1}, $F_V = 6.28(0.75) \times 10^{-2}$ m^2 C^{-1}, and $F_D = 6.19(0.76)$ m$^{3/2}$ J$^{-1/2}$. These maximum values correspond nicely to the changes in phase fractions shown in Fig. 2. Due to a purely monoclinic phase for a low Si content, the corresponding samples exhibit a non-polar character. The maximum polar orthorhombic phase fraction between 1.9 at% and 2.5 at% Si is the reason for the maximum of the polar properties. The strongly constricted hysteresis with a non-zero remanent polarization for Si concentrations of 2.5 at% and 3.5 at% stems from a

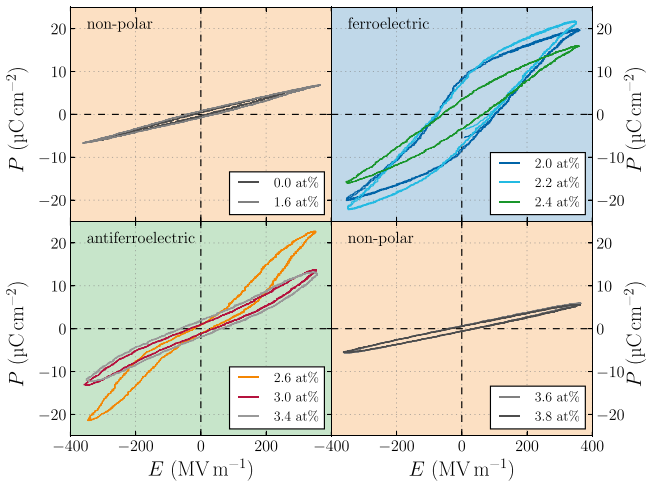

FIG. 1. Hysteresis of non-polar (top left and bottom right), ferroelectric (top right), and antiferroelectric (bottom left) Si:HfO$_2$, depending on the Si concentration. The hysteresis loops were measured by the shunt method using a triangular voltage sweep of amplitude 3.5 V and frequency 1 kHz at room temperature.

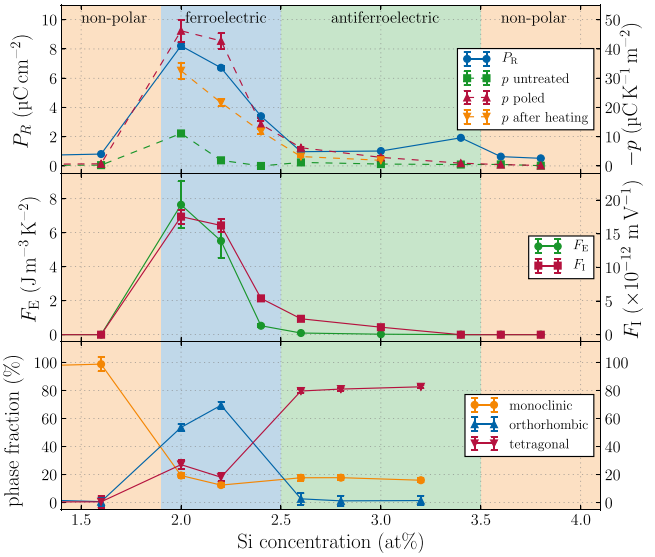

FIG. 2. Top: Remanent polarization P_R and pyroelectric coefficient p. Middle: Exemplary figures of merit F_E and F_I for energy harvesting and IR sensor applications. Bottom: Fitted fractions of individual phases depending on Si incorporation obtained by Rietveld refinement according to Ref. 8.

mixture of the tetragonal and monoclinic phases. It seems that the tetragonal phase gives rise to antiferroelectric behavior. While nearly all samples show a negligible pyroelectric coefficient in the unpoled state, i.e., before an initial *P–E* measurement, a pyroelectric coefficient of approx. $-10\,\mu C\,K^{-1}\,m^{-2}$ can be measured using the Sharp-Garn method for a Si concentration of 2.0 at%. This is an indication for aligned domains, already established by the fabrication process. The origin of this phenomenon is still unclear and, thus, needs further investigation, such as TEM studies of grain orientations or X-ray texture measurements.

The highest p value for 2.0 at% Si in HfO_2 is quite similar to the recently published values of Smith *et al.* for 20 nm thick $Hf_{1-x}Zr_xO_2$ layers, where a maximum pyroelectric coefficient of $48\,\mu C\,K^{-1}\,m^{-2}$ was determined at a composition of $x = 0.64$. Compared to other well-known ferro- and pyroelectrics, the values of p at room temperature are larger than those for single crystal III-V compound semiconductors, such as GaN[37,38] and AlN,[39,40] and similar to organic semi-crystalline polymers like polyvinylidene fluoride (PVDF)[41] and its copolymer with trifluoroethylene [P(VDF-TrFE)].[41,42] Inorganic perovskite-type single crystals, e.g., $LiNbO_3$[43] and $LiTaO_3$ (Ref. 43), as well as lead-based materials, e.g., modified lead zirconate titanate ceramics and thin films,[44–46] and solid solutions of lead magnesium niobate-lead titanate (PMN-PT)[47,48] provide much higher pyroelectric coefficients. Comparing the maximum F_I values [more relevant than F_V for small area elements with comparably low ε_r (Ref. 45)], it is found that a similar tendency as for p is present. In contrast to industry leading $LiTaO_3$ single crystals, Si:HfO_2 provides only a third of its F_I and half of its F_V. The exact values of all mentioned materials are given in supplementary material SIII. While the thin film processing of ferroelectric materials can be quite complex, the fabrication of HfO_2 thin films is comparably easy and already well established for CMOS applications. Additionally, the readout chip might be processed on the same silicon substrate. Nonetheless, it should be kept in mind that this is just a first assessment without years of intensive optimizations as for other materials. Necessary additional considerations include thermal time constants, low thermal conductance, and matching capacity between the detector element and the attached amplifier chip, all of which are important factors to optimize IR sensors.[45]

The $p(T)$ curves determined using the Sharp-Garn method for ferro- and antiferroelectric Si:HfO_2 are shown in Fig. 3, revealing varying temperature dependencies of P_R for different Si doping concentrations. A Si concentration of 2.0 at% has an almost constant $p(T)$ behavior in the investigated temperature range. For larger Si concentrations, the absolute pyroelectric coefficient drops to lower absolute values and slightly decreases with increasing temperature, which is in accordance with previous results.[22] Although $|p|$ generally increases close to a phase transition, the decreasing behavior may stem from the grain size effect mentioned by Hoffmann *et al.*.[22] Smaller grains have a lower transition temperature and, thus, get depolarized at lower temperatures. The fact that $|p|$ at room temperature after poling is always lower after a heating step (see Fig. 2) supports this. Another explanation could be the increased internal bias field caused

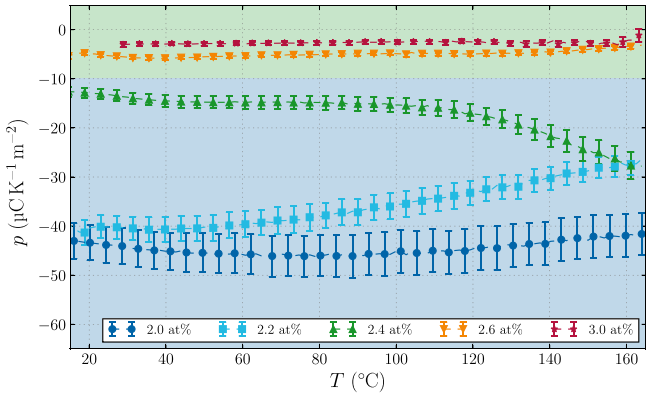

FIG. 3. Pyroelectric coefficient as a function of temperature $p(T)$ for different Si concentrations in HfO_2.

by charge redistribution, which lowers P_R and thus p after heating the material.[49–51] The Si concentration of 2.4 at%, which is close to the transition from the ferro- to the antiferroelectric phase, is an exception to this general trend. Here, $|p|$ increases with increasing temperature, which indicates a temperature-driven transition from the ferro- to the antiferroelectric phase so that P_R varies more and, thus, $|p|$ increases. For Si concentrations above 2.5 at%, marked by antiferroelectric behavior and low P_R, $|p|$ remains nearly constant at relatively low absolute values for the complete investigated temperature range. A Curie temperature, i.e., phase change temperature to a non-polar phase, was not detected from the $p(T)$ measurements, and thus, a temperature-induced phase transition is not present in the investigated temperature range. The initial value of p can be recovered by poling the sample again.

Pyroelectric coefficients obtained from a continuous electric field-cycling method may be much higher than those obtained by a method with absent electric field, as recently shown in Si:HfO_2.[22] A possible explanation could be different degrees of polarization of the films at different temperatures. Typical hysteresis loops of Si:HfO_2 show no complete polarization (see Fig. 1 and Refs. 22 and 25), i.e., the maximum electric field before breakdown is not sufficient to completely polarize the thin films. This can be seen from hysteresis measurements with the increasing electric field amplitude, which give an increasing P_R with the field.[21] The obtainable fraction of the full polarization may further depend on temperature, despite the use of equal field amplitudes. Calculating the pyroelectric coefficient from such data means to use only a temperature-dependent fraction of the full P_R so that the maximum achievable p can actually be higher. In contrast to that, field-free methods start from an initial polarization value without changing this polarization state during the temperature variation.

By integrating the obtained $p(T)$ data and adding the value of P_R at room temperature (obtained from hysteresis measurements), the remanent polarization dependency can be reconstructed. The absolute change and absolute value of the remanent polarization, $\Delta P_R^*(T)$ and P_R^*, without the use of an external electric field for their determination are summarized in Fig. 4, respectively. P_R^* is marked with an asterisk because the different degree of polarization at different temperatures obtained from a hysteresis measurement may differ from that

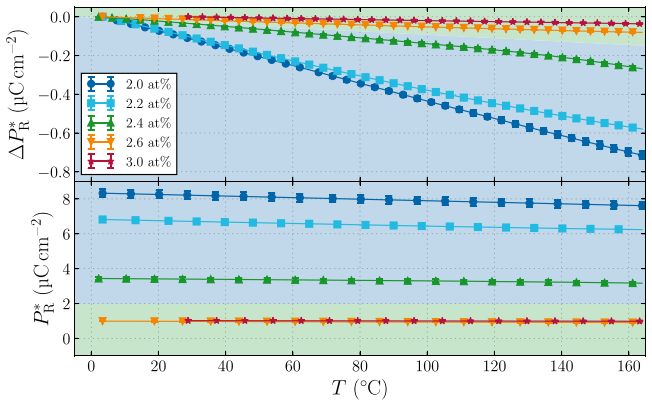

FIG. 4. Top: Absolute change in the remanent polarization ΔP_R^* with respect to temperature T calculated by integrating the data of Fig. 3. Bottom: Absolute value of P_R^* using the room temperature values from Fig. 2 as the offset.

of a temperature-dependent pyroelectric coefficient measurement. The slight change in P_R^* is nearly linear with T, corresponding to the almost temperature-invariant p for all Si concentrations. The largest variance of P_R^* is again present for the most polar 2.0 at% sample, caused by the largest pyroelectric coefficient. Here, P_R^* changes by approx. 13% over the temperature range of 170 K. All other concentrations show a smaller absolute change in P_R^* with temperature, accompanied by smaller absolute values of P_R^* and p (see the bottom of Fig. 4). Compared to the absolute value of P_R^*, the change ΔP_R^* is quite small, leaving P_R^* quasi-constant with T. This is not necessarily expected from Si:HfO_2 as it is considered as a rather "fragile" system due to its smaller concentration window for ferroelectric properties compared to other dopants and its related increased sensitivity to the impact of the grain size and oxygen vacancies.[25] However, its ferro- and pyroelectric properties remain relatively stable between ambient and elevated temperatures. This is especially promising for future applications and device manufacturing.

In conclusion, dynamic P–E hysteresis measurements and the electric field-free determination of the pyroelectric coefficient p were used to correlate the polar properties with the phase fractions of silicon-doped HfO_2. Pronounced ferro- and pyroelectric properties emerge for Si concentrations between 1.9 at% and 2.5 at%. Maximum values of $p = -46.2(6.1)$ μC K^{-1} m^{-2} and $P_R = 8.21(0.22)$ μC cm^{-2} were found for a Si concentration of 2.0 at%. A good correlation between the orthorhombic phase fraction and the pronounced polar properties is shown. Deviations from previously published values of p by measuring temperature-dependent hysteresis loops likely stem from an incomplete polarization. Temperature-dependent measurements of p in the range of 0 °C to 170 °C reveal a nearly constant behavior of the pyroelectric coefficient and remanent polarization. Compared to other dopants, a stable ferroelectric phase is harder to establish in silicon-doped HfO_2, but its polarization changes only little in the typical operation temperature range of a potential device. This, together with the well-established fabrication process, makes it a promising candidate for integrated device applications including sensors utilizing the pyroelectric effect.

See supplementary material for further details of the raw signals of the current and temperature course, measurements of ε_r, and calculations and comparisons of figures of merit.

Parts of this work have been carried out in the project "Nutzung von Abwärme zur Erzeugung von Wasserstoff und Elektrizität mit pyroelektrischen Oxiden" (No. 100245339) financially supported by the Sächsische Aufbaubank. T. Schenk gratefully acknowledges the German Research Foundation (Deutsche Forschungsgemeinschaft) for funding part of this research in the frame of the "Inferox" Project (No. MI 1247/11-2). M. H. Park was supported by a Humboldt postdoctoral fellowship of the Alexander von Humboldt foundation.

[1]T. S. Böscke, J. Müller, D. Bräuhaus, U. Schröder, and U. Böttger, Appl. Phys. Lett. **99**, 102903 (2011).
[2]M. H. Park, Y. H. Lee, H. J. Kim, Y. J. Kim, T. Moon, K. D. Kim, J. Müller, A. Kersch, U. Schroeder, T. Mikolajick, and C. S. Hwang, Adv. Mater. **27**, 1811 (2015).
[3]S. Flachowsky, T. Mikolajick, S. Müller, T. Schenk, E. Yurchuk, S. Slesazeck, U. Schröder, R. van Bentum, S. Kolodinski, P. Polakowski, and J. Müller, in *6th Forum on New Materials - Part C*, Advances in Science and Technology Vol. 95 (Trans Tech Publications, 2014), pp. 136–145.
[4]J. Müller, P. Polakowski, S. Mueller, and T. Mikolajick, ECS J. Solid State Sci. Technol. **4**, N30 (2015).
[5]T. Schenk, M. Hoffmann, C. Richter, M. Pešić, S. Mueller, S. Slesazeck, U. Schroeder, T. Mikolajick, D. Pohl, J. Mueller, P. Polakowski, R. Materlik, A. Kersch, X. Sang, E. D. Grimley, and J. M. LeBeau, in *MRS Fall Meeting*, Boston, MA (2015), pp. 1–47.
[6]J. Van Houdt, in *2017 IEEE International Memory Workshop (IMW)* (IEEE, 2017), pp. 1–3.
[7]X. Tian and A. Toriumi, in *2017 IEEE Electron Devices Technology and Manufacturing Conference (EDTM)* (IEEE, 2017), pp. 36–64.
[8]M. H. Park, T. Schenk, C. M. Fancher, E. D. Grimley, C. Zhou, C. Richter, J. M. LeBeau, J. L. Jones, T. Mikolajick, and U. Schroeder, J. Mater. Chem. C **5**, 4677 (2017).
[9]T. Schenk, M. Pesic, M. H. Park, M. Hoffmann, H. Mulaosmanovic, C. Richter, F. P. G. Fengler, S. Slesazeck, U. Schroeder, S. Mueller, and T. Mikolajick, in *Toward Oxide-Based Electronics, Spring Meeting*, Luxembourg (2017), pp. 1–40.
[10]S. Starschich and U. Boettger, J. Mater. Chem. C **5**, 333 (2017).
[11]T. C. U. Tromm, J. Zhang, J. Schubert, M. Luysberg, W. Zander, Q. Han, P. Meuffels, D. Meertens, S. Glass, P. Bernardy, and S. Mantl, Appl. Phys. Lett. **111**, 142904 (2017).
[12]S. Zarubin, E. Suvorova, M. Spiridonov, D. Negrov, A. Chernikova, A. Markeev, and A. Zenkevich, Appl. Phys. Lett. **109**, 192903 (2016).
[13]S. Starschich, D. Griesche, T. Schneller, R. Waser, and U. Böttger, Appl. Phys. Lett. **104**, 202903 (2014).
[14]S. Mueller, J. Mueller, A. Singh, S. Riedel, J. Sundqvist, U. Schroeder, and T. Mikolajick, Adv. Funct. Mater. **22**, 2412 (2012).
[15]S. Mueller, C. Adelmann, A. Singh, S. Van Elshocht, U. Schroeder, and T. Mikolajick, ECS J. Solid State Sci. Technol. **1**, N123 (2012).
[16]P. D. Lomenzo, Q. Takmeel, C. Zhou, C.-C. Chung, S. Moghaddam, J. L. Jones, and T. Nishida, Appl. Phys. Lett. **107**, 242903 (2015).
[17]D. Lehninger, D. Rafaja, J. Wünsche, F. Schneider, J. von Borany, and J. Heitmann, Appl. Phys. Lett. **110**, 262903 (2017).
[18]S. Starschich and U. Böttger, J. Appl. Phys. **123**, 044101 (2018).
[19]P. Polakowski, S. Riedel, W. Weinreich, M. Rudolf, J. Sundqvist, K. Seidel, and J. Müller, in *2014 IEEE 6th International Memory Workshop (IMW)* (IEEE, 2014), pp. 1–4.
[20]S. Starschich, T. Schenk, U. Schroeder, and U. Boettger, Appl. Phys. Lett. **110**, 182905 (2017).
[21]S. W. Smith, A. R. Kitahara, M. A. Rodriguez, M. D. Henry, M. T. Brumbach, and J. F. Ihlefeld, Appl. Phys. Lett. **110**, 072901 (2017).
[22]M. Hoffmann, U. Schroeder, C. Künneth, A. Kersch, S. Starschich, U. Böttger, and T. Mikolajick, Nano Energy **18**, 154 (2015).
[23]M. H. Park, H. J. Kim, Y. J. Kim, T. Moon, K. Do Kim, and C. S. Hwang, Nano Energy **12**, 131 (2015).
[24]S. Jachalke, E. Mehner, H. Stöcker, J. Hanzig, M. Sonntag, T. Weigel, T. Leisegang, and D. Meyer, Appl. Phys. Rev. **4**, 021303 (2017).

[25]C. Richter, T. Schenk, M. H. Park, F. A. Tscharntke, E. D. Grimley, J. M. LeBeau, C. Zhou, C. M. Fancher, J. L. Jones, T. Mikolajick, and U. Schroeder, Adv. Electron. Mater. **106**, 1700131 (2017).
[26]C. Mart, T. Kämpfe, S. Zybell, and W. Weinreich, Appl. Phys. Lett. **112**, 052905 (2018).
[27]T. Schenk, E. Yurchuk, and S. Mueller, Appl. Phys. Rev. **1**, 041103 (2014).
[28]N. Menou, C. Muller, I. S. Baturin, V. Y. Shur, and J. L. Hodeau, J. Appl. Phys. **97**, 064108 (2005).
[29]D. Zhou, J. Xu, Q. Li, Y. Guan, F. Cao, X. Dong, J. Müller, T. Schenk, and U. Schröder, Appl. Phys. Lett. **103**, 192904 (2013).
[30]T. Schenk, U. Schroeder, M. Pešić, M. Popovici, Y. V. Pershin, and T. Mikolajick, ACS Appl. Mater. Interfaces **6**, 19744 (2014).
[31]T. Schenk, M. Hoffmann, J. Ocker, M. Pešić, T. Mikolajick, and U. Schroeder, ACS Appl. Mater. Interfaces **7**, 20224 (2015).
[32]L. E. Garn and E. J. Sharp, J. Appl. Phys. **53**, 8974 (1982).
[33]L. E. Garn and E. J. Sharp, J. Appl. Phys. **53**, 8980 (1982).
[34]N. Setter, Ferroelectrics **500**, 164 (2016).
[35]C. Kittel, Phys. Rev. **82**, 729 (1951).
[36]M. Hoffmann, T. Schenk, M. PeŠić, U. Schroeder, and T. Mikolajick, Appl. Phys. Lett. **111**, 182902 (2017).
[37]S. Jachalke, P. Hofmann, G. Leibiger, F. S. Habel, E. Mehner, T. Leisegang, D. C. Meyer, and T. Mikolajick, Appl. Phys. Lett. **109**, 142906 (2016).
[38]K. Matocha, T. P. Chow, and R. J. Gutmann, IEEE Electron Device Lett. **23**, 79 (2002).
[39]Y. V. Shaldin and S. Matyjasik, Semiconductors **45**, 1117 (2011).
[40]V. Fuflyigin, E. Salley, A. Osinsky, and P. Norris, Appl. Phys. Lett. **77**, 3075 (2000).
[41]A. J. Lovinger, Science **220**, 1115 (1983).
[42]E. Mehner, S. Jachalke, J. Hanzig, T. Leisegang, H. Stöcker, and D. C. Meyer, Ferroelectrics **510**, 132 (2017).
[43]S. B. Lang, Phys. Today **58**(8), 31 (2005).
[44]Q. Zhang and R. W. Whatmore, J. Appl. Phys. **94**, 5228 (2003).
[45]R. W. Whatmore, A. Patel, N. M. Shorrocks, and F. W. Ainger, Ferroelectrics **104**, 269 (1990).
[46]B. Ploss and S. Bauer, Sens. Actuators A **26**, 407 (1991).
[47]G. Sebald, L. Seveyrat, D. Guyomar, L. Lebrun, B. Guiffard, and S. Pruvost, J. Appl. Phys. **100**, 124112 (2006).
[48]Y. Tang, X. Wan, X. Zhao, X. Pan, D. Lin, H. Luo, J. Sun, X. Meng, and J. Zhu, J. Appl. Phys. **98**, 084104 (2005).
[49]F. P. G. Fengler, S. Slesazeck, T. Mikolajick, and U. Schroeder, Adv. Electron. Mater. **4**(3), 1700547 (2018).
[50]E. D. Grimley, T. Schenk, X. Sang, M. Pešić, U. Schroeder, T. Mikolajick, and J. M. LeBeau, Adv. Electron. Mater. **2**, 1600173 (2016).
[51]M. Pešić, F. P. G. Fengler, L. Larcher, A. Padovani, T. Schenk, E. D. Grimley, X. Sang, J. M. LeBeau, S. Slesazeck, U. Schroeder, and T. Mikolajick, Adv. Funct. Mater. **26**, 4601 (2016).